



Highly productive and robust core@shell HeatPath SiC-Al₂O₃ @Co/Re/Al₂O₃ catalyst for Fischer–Tropsch synthesis

Rui Zhang^{a,1}, Junrui Li^{a,*}, Anna Lee Tonkovich^b, Cody Lockhart^c, Xiaoyan Wang^c, Wenda Hu^a, Hafsa Karroum^a, Matthew Seabaugh^c, Norbert Kruse^{a,d,*}, Yong Wang^{a,d,*}

^a Voiland School of Chemical Engineering and Bioengineering, Washington State University, Pullman, WA 99164-6515, United States

^b Tonkomo, LLC, Gilbert, AZ 85297, United States

^c Nexceris LLC, Lewis Ctr, OH, United States

^d Institute for Integrated Catalysis, Pacific Northwest National Laboratory, Richland, WA 99332, United States

ARTICLE INFO

Keywords:

Fischer–Tropsch synthesis
Core@shell structure
Cobalt catalyst
Temperature control
C₅₊ hydrocarbon
Methane selectivity

ABSTRACT

Co-based catalysts are highly active for synthesizing long-chain paraffins through Fischer–Tropsch synthesis. However, their exothermic reactions can cause overheating and catalyst deactivation. To address this, thermally conductive SiC-Al₂O₃ pellets (HeatPath™) were coated with a Co/Re/Al₂O₃ shell, significantly boosting the CO conversion rate and the yield of C₂₋₄ and C₅₊ hydrocarbons over a wide range of temperatures by dissipating the reaction heat. The core@shell HeatPath@Co/Re/Al₂O₃ catalyst demonstrated high productivity (up to 19.7 g_{CO} g_{cat}⁻¹ h⁻¹), exceptional long-term stability over 660 h time-on-stream, with high-temperature operation up to 260 °C, a low CH₄ selectivity (7.1 %) and a chain growth probability (α) > 0.8. In contrast, the irreversible deactivation of a powder Co/Re/Al₂O₃ catalyst started at 195 °C, resulting in >60 % CH₄ selectivity and ~100 % CO conversion due to excessive local heat. The CO conversion rate on the core@shell catalyst could be further improved by increasing the H₂/CO ratio and temperature, with commercially viable CH₄ selectivity.

1. Introduction

Fischer–Tropsch synthesis (FTS) is a promising method for producing eco-friendly fuels and industrial chemicals, including alkanes, alkenes, alcohols, aldehydes, or their mixture [1–8]. Of the various FTS catalysts, cobalt (Co)-based materials are widely studied due to their high activity, low CH₄ selectivity, low tendency for the intrinsic water-gas shift reaction (WGS, CO+H₂O=CO₂+H₂), and ability to produce long-chain paraffins [9–12]. However, the exothermic nature of the FTS reaction, combined with the high activity of cobalt-based catalysts, can lead to localized overheating. Hot spots result in deactivation of the Co-based catalysts due to cobalt particle agglomeration [8], surface reconstruction [13], and metal-support reactions [14]. Hence, effective temperature control is crucial for enhancing the stability of cobalt-based catalysts.

Fixed bed, fluidized bed, and slurry bubble column reactors are frequently used for FTS [15–17]. Recently, microchannel reactors have been employed for FTS due to their excellent heat transfer and temperature control [18,19]. Our previous research has demonstrated the

potential of microchannel reactors, as they achieved a high single-pass CO conversion (60 %) under a high gas hourly space velocity (60,000 h⁻¹) on a Co/Re/Al₂O₃ catalyst through improved mass transfer and temperature control [19,20]. However, improving catalyst performance in existing FTS reactors remains a challenging task.

An alternative approach to controlling the temperature in FTS is to use support materials with high thermal conductivity. Using metal foams as supports for Co/Al₂O₃ catalysts has been shown to improve C₅₊ selectivity while reducing CH₄ selectivity compared to powder Co/Al₂O₃ catalysts [21–23]. The Co-coated metallic foams described by Park [21] improved performance over powders but demonstrated modest catalyst productivity (1.13 g_{CO} g_{cat}⁻¹ h⁻¹) of more than an order of magnitude below the exemplar HeatPath catalysts described herein in large part due to inferior heat transfer of foams with a high void volume [24,25], compared to pellets with a high thermal conductivity. Further, the low specific surface area of metal foams results in poor active phase dispersion [26] which limits their industrial applications.

* Corresponding authors at: Voiland School of Chemical Engineering and Bioengineering, Washington State University, Pullman, WA 99164-6515, United States. E-mail addresses: junrui.li@wsu.edu, jli@cau.edu (J. Li), norbert.kruse@wsu.edu (N. Kruse), wang42@wsu.edu (Y. Wang).

¹ These authors contributed equally to this work.

² Department of Chemistry, Clark Atlanta University, Atlanta, GA, 30314, United States.

Silicon carbide is another commonly studied support material due to its superior thermal conductivity ($120 \text{ W m}^{-1} \text{ K}^{-1}$ as compared to $1.4 \text{ W m}^{-1} \text{ K}^{-1}$ for SiO_2 and to $20\text{--}35 \text{ W m}^{-1} \text{ K}^{-1}$ for Al_2O_3), chemical inertness, rich surface oxygen groups, and mechanical stability [27]. Using porous silicon carbide or foam as a support has been shown to result in high activity, high C_{5+} selectivity, and high chain growth probability (α) at temperatures as high as 240°C [28–31], but the synthesis of those structures can be complex, limiting their practical utilization.

Here, we have introduced an efficient method for controlling FTS temperature by using a HeatPath $\text{SiC-Al}_2\text{O}_3 @\text{Co/Re/Al}_2\text{O}_3$ with core@shell structure. The packed bed using high thermal conductivity pellets effectively dissipates excess heat generated during the reaction to maintain the high activity and dispersion of Co nanoparticles. To demonstrate this, we coated a thin layer of the highly active Co/Re/ Al_2O_3 catalyst [19] ($20\text{--}30 \mu\text{m}$) on commercially available SiC-composite pellets. Our results showed that the core@shell structure of HeatPath $\text{SiC-Al}_2\text{O}_3 @\text{Co/Re/Al}_2\text{O}_3$ not only dramatically improved the CO conversion rate up to 260°C , but also prevented high-temperature runaway that was observed for a powder catalyst of identical formulation at temperatures near 195°C . Furthermore, characterization of fresh and spent catalysts by TEM, Raman, and XRD showed that the HeatPath $\text{SiC-Al}_2\text{O}_3$ pellet-based core@shell structure retained the good dispersion of ultrafine Co nanoparticles, unlike the sintered Co nanoparticles in the powder catalyst.

2. Experimental section

2.1. Catalyst preparation

2.1.1. Materials and chemicals

Alumina support (98 % Al_2O_3 , PURALOXTH®100/150 L4) was obtained from Sasol. $\text{Co}(\text{NO}_3)_2 \cdot 6 \text{H}_2\text{O}$ (98 %) and perrenic acid (HReO_4 , 75–80 wt% in H_2O) were purchased from Sigma-Aldrich and used as received. HeatPath pellets were obtained from Nexceris in a pressed pellet form with a 6-mm diameter and 4-mm height. The HeatPath pellet core is substantially dense and is a composite of SiC and Alumina. The core is further hermetically protected with a thin layer of alpha-alumina (AlumiLok™) that protects SiC from corrosion and is rough to improve subsequent active shell catalyst coating uniformity and long-term adhesion. The experimentally measured thermal conductivity of the dense composite $\text{SiC-Al}_2\text{O}_3$ HeatPath core structure under FTS operating conditions is about $12 \text{ W m}^{-1} \text{ K}^{-1}$ as compared to $20 \text{ W m}^{-1} \text{ K}^{-1}$ at room temperature.

2.1.2. Preparation of catalyst on pellets

The Al_2O_3 support (PURALOXTH 100/150 L4,) was pre-calcined at 500°C in air for 2 h and stored in a desiccator. In a typical procedure, 46 g $\text{Co}(\text{NO}_3)_2 \cdot 6 \text{H}_2\text{O}$ and 1.1 ml HO_4Re solution were dissolved in 22 ml H_2O as a stock solution. 8 ml stock solution was added to 20 g pre-calcined Al_2O_3 support via an incipient wetness impregnation method, followed by drying at 90°C for 8 h and calcination at 350°C for 3 h in air. The same procedure was repeated twice with 7 ml stock solution added to the solid mixture each time until all the stock solution was used. The obtained powder was denoted as Co/Re/ Al_2O_3 with the nominal weight loading of Co and Re being 30.3 wt%, and 4.8 wt%, respectively. To prepare the catalyst slurry, 3 g of the Co/Re/ Al_2O_3 was ball-milled with 17 ml water for 3 h. No binding or stabilizing materials were added to the slurry. Pellet was then dip-coated in the slurry and dried at 80°C to form a thin and uniform coating. The dip-coating process was repeated 6 times to obtain a loading of $\sim 5.5 \text{ mg}$ of catalyst per pellet. The core@shell HeatPath $\text{SiC-Al}_2\text{O}_3 @\text{Co/Re/Al}_2\text{O}_3$ pellet was then calcined at 550°C for 4 h in air after ramping the rate at $5^\circ\text{C}/\text{min}$.

2.2. Catalyst characterization

X-ray diffraction (XRD) was performed on powder samples using the Rigaku Miniflex 600 diffractometer at a speed of $0.5 \text{ deg}/\text{min}$. Raman spectra were performed using a Horiba LabRAM HR microscope system integrated with a Ventus LP 532 laser (532 nm). Transmission electron microscopy (TEM) was conducted using the FEI Technai G2 20 Twin TEM at 200 kV. Scanning electron microscopy (SEM) was performed with integrated energy dispersive X-ray spectroscopy (EDS) using a TESCAN VEGA3 at 1153x magnification and 25 kV. The fresh catalysts were used for characterizations after the calcination and before the in-situ redox treatment. For evaluation of the spent catalysts, catalysts on pellets were sonicated in water before being dried up at 80°C , and those powder catalysts were separated from SiC powder by sifting them out for further characterizations.

2.3. Catalytic evaluations

The Fischer–Tropsch (F–T) reactions were carried out in a fixed-bed reactor consisting of a quartz tube with an inner diameter of 7 mm that was placed at the center of a stainless-steel housing when operating at high pressure. The catalyst loading was typically 0.5 g for the powdered catalysts ($0.125\text{--}0.25 \text{ mm}$) that was mixed with 1 g SiC powder, and twenty core@shell HeatPath $\text{SiC-Al}_2\text{O}_3 @\text{Co/Re/Al}_2\text{O}_3$ pellets (with a total of 0.1108 g Co/Re/ Al_2O_3 catalyst, respectively. And individual pellet weights noted in Table S1). The activation of the catalyst was conducted in a tube furnace with two redox cycles, each of which consisted of two steps: 1) reduction of catalyst with 10% H_2 in N_2 at 1 bar (50 ml/min (STP)) by ramping the temperature from room temperature to 250°C at $0.5^\circ\text{C}/\text{min}$, holding at 250°C for 30 min, and then ramping to 400°C at $0.5^\circ\text{C}/\text{min}$ and holding for 10 h, followed by purging with N_2 during cooling to room temperature; 2) oxidizing the catalyst with 1 % O_2 in N_2 at 1 bar (50 ml/min (STP)) by ramping the temperature at a rate of $2^\circ\text{C}/\text{min}$ up to 350°C and holding for 2 h, followed by cooling to room temperature in flowing N_2 . After repeating the above two steps to complete two redox cycles, the catalysts were transferred to the isothermal region of the reactor, and the final reduction was carried out in-situ with H_2 at 1 bar (25 ml/min (STP)) at 400°C for 12 h after applying a ramping rate of $0.5^\circ\text{C}/\text{min}$. Next, the temperature was reduced to 160°C , and the total pressure was raised to 20 bar in the presence of H_2 before switching to a mixture of H_2 and CO. (Note that the reported pressure in this work refers to gauge pressure). The target reaction temperature was approached with a heating rate of $0.1^\circ\text{C}/\text{min}$. Catalytic activity and product selectivity were measured for at least 12 h time-on-stream (TOS) at each test condition after the system reached the steady state (roughly after 100 h of operation), using chromatography-mass spectrometry equipped with two sampling loops (GC–MS, Agilent 7890A-5975). The GC/MS system and the outlet of the reactor were connected through a capillary which was maintained at 200°C by a heating tape to avoid condensation of heavy products. Light gases (up to C_3) were determined by a thermal conductivity detector (TCD) with two connected columns of 3 Foot and 9 Foot Hayesep Q 80/100 (in backflush mode), while C_{4+} hydrocarbons and alcohols were analyzed by an MS detector with the DB-1 capillary column [28].

Using our GC-MS system (Agilent 7890A-5975), quantitative analysis of paraffins was performed on the C_{1-12} fraction. The chain lengthening probabilities (alpha numbers) for paraffins were calculated for C_{4-8} . C_{1-3} fractions were not considered since they showed strong deviations from the Anderson-Schulz-Flory distribution, consistent with what was observed in the literature [32]. Fig. S1,a shows that the analysis of liquid samples (collected at reaction conditions of 235°C $\text{H}_2/\text{CO}=1.65$, 245°C $\text{H}_2/\text{CO}=1.8$, 255°C $\text{H}_2/\text{CO}=1$) confirmed the presence of hydrocarbons up to C_{32} , so a linear extrapolation for paraffins to C_{13-32} was performed using the alpha numbers (α)

calculated from C_{4-8} products. The alpha numbers were calculated based on the Anderson-Schulz-Flory equation $W_n = n(1 - \alpha)^2 \alpha^{n-1}$ where W_n stands for the mass fraction of products containing n carbon atoms. Figs. S1, b-d show that alpha numbers for paraffins calculated from C_{5-32} of liquid samples agree reasonably well with the alpha numbers for paraffins calculated from C_{4-8} of gas samples. The carbon mole balance was used to determine the CO conversion and the hydrocarbon selectivities.

The CO conversion X_{CO} was calculated using Eq. (1).

$$X_{CO}(\%) = \frac{\sum [carbon]_i}{[CO]_{out} + \sum [carbon]_i} \quad (1)$$

Where $\sum [carbon]_i = 1 \times ([CH_4]_{out} + [CH_3OH]_{out}) + 2 \times ([C_2H_6]_{out} + [C_2H_4]_{out} + [C_2H_5OH]_{out}) + 3 \times ([C_3H_8]_{out} + [C_3H_6]_{out} + [C_3H_7OH]_{out}) + \dots$, reflecting the total carbon molar concentration of hydrocarbon and alcohol products in the outlet gas. $[CO]_{out}$ represents the carbon molar concentration of unconverted CO in the outlet gas.

The C_n selectivity was calculated using Eq. (2).

$$S_{C_n}(\%) = \frac{n \times [C_n]_{out}}{\sum [carbon]_i}, \quad (2)$$

where n and $[C_n]_{out}$ are the number of carbon atoms and the molar concentration of species C_n in the outlet gas, respectively.

The CO conversion rate (r_{CO} , $g_{CO} g_{cat}^{-1} h^{-1}$) was calculated using Eq. (3).

$$r_{CO} = \frac{X_{CO} \times V_{CO.in}}{g_{catalyst}} \quad (3)$$

where X_{CO} is the CO conversion and $V_{CO.in}$ is the inlet mass flow rate of CO (gh^{-1}).

The space time yield (STY) of products (STY, $mg g_{cat}^{-1} h^{-1}$) is defined as Eq. (4).

$$STY = \frac{X_{CO} \times N_{CO.in} \times S_{C_n} \times M_w}{g_{catalyst} \times n} \quad (4)$$

where X_{CO} is the CO conversion, $N_{CO.in}$ is the inlet mass flow rate of CO ($mmolh^{-1}$), S_{C_n} and M_w represent the selectivity and molecular weight of the product, respectively, and n is the number of carbon atoms in the products.

3. Results and discussion

3.1. Structural and morphological study

Electron microscopy imaging (Transmission electron microscopy (TEM) and scanning electron microscopy (SEM)) were used to study the structure and morphology of the HeatPath catalyst in comparison to the powder Co/Re/Al₂O₃ catalyst. As shown in Fig. 1, TEM analysis indicates a similar size and morphology of Co/Re/Al₂O₃ in both the fresh HeatPath coated catalyst (Fig. 1a, circled black region indicates the Co particles) and powder (Fig. 1c) catalysts with no redox treatment. In both cases, the Co/Re/Al₂O₃ domains mostly consisted of Co nanoparticles or agglomerates of various sizes. The Co nanoparticles in the HeatPath SiC-Al₂O₃ @Co/Re/Al₂O₃ catalyst maintained their ultrafine size of less than 2 nm after 600 h time-on-stream (TOS) in the FTS reaction, as seen in Fig. 1b. In contrast, Co in the powder catalyst experienced significant sintering and growth in particle size, as demonstrated in Fig. 1d. The size distribution of the Co nanoparticles in spent HeatPath catalysts and the spent powder catalysts is shown in Fig. S2. The results suggest that the SiC support (pellet) effectively dissipated heat generated through the reaction, thus preventing the Co nanoparticles from sintering during the FTS reaction. Additionally, the energy dispersive spectroscopy (EDX) mapping of the spent HeatPath catalyst in Fig. 1e displays an even distribution of Co, Re, and Al species throughout the surface of the SiC pellet.

3.2. Comparison of catalytic performance between HeatPath and powder catalysts

As shown in Fig. 2a, the performance of both powder and HeatPath catalysts was compared at 195 °C and 20 bar after time-on-stream

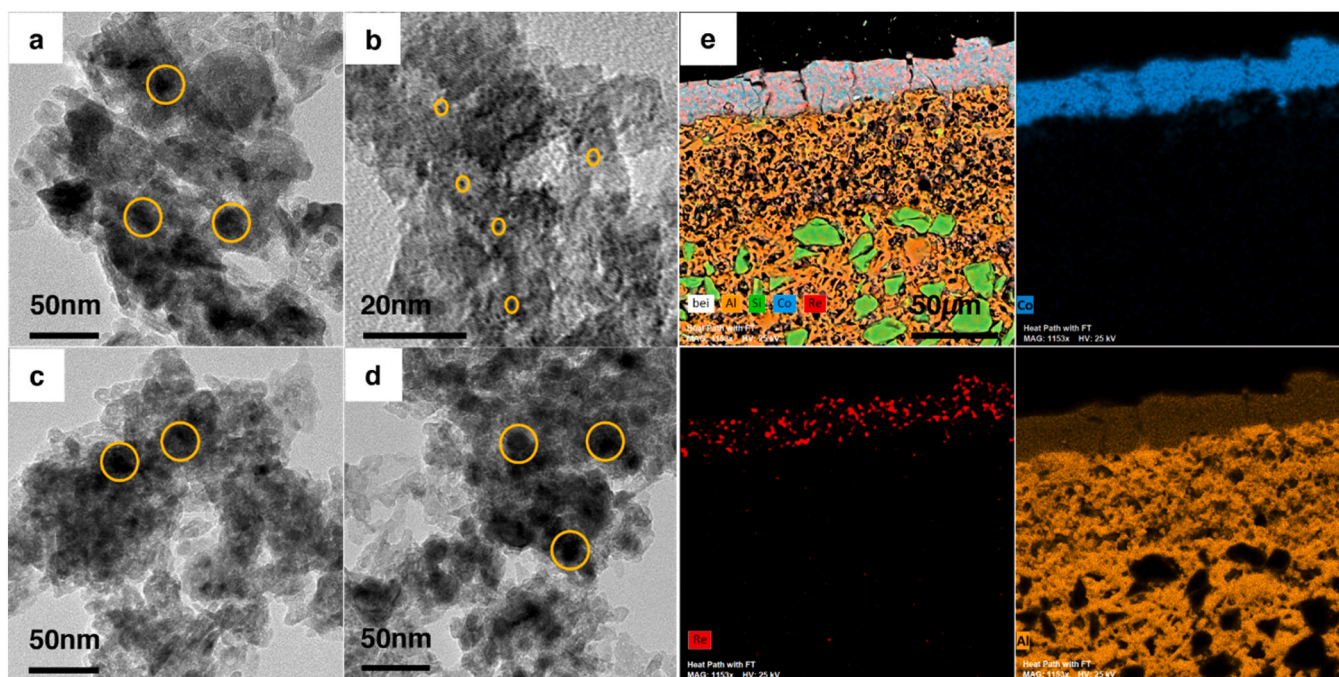


Fig. 1. TEM images of fresh and spent (a,b) HeatPath SiC-Al₂O₃ @Co/Re/Al₂O₃ and (c,d) powder Co/Re/Al₂O₃ catalysts. (e) EDX Mapping images of spent HeatPath SiC-Al₂O₃ @Co/Re/Al₂O₃ catalyst.

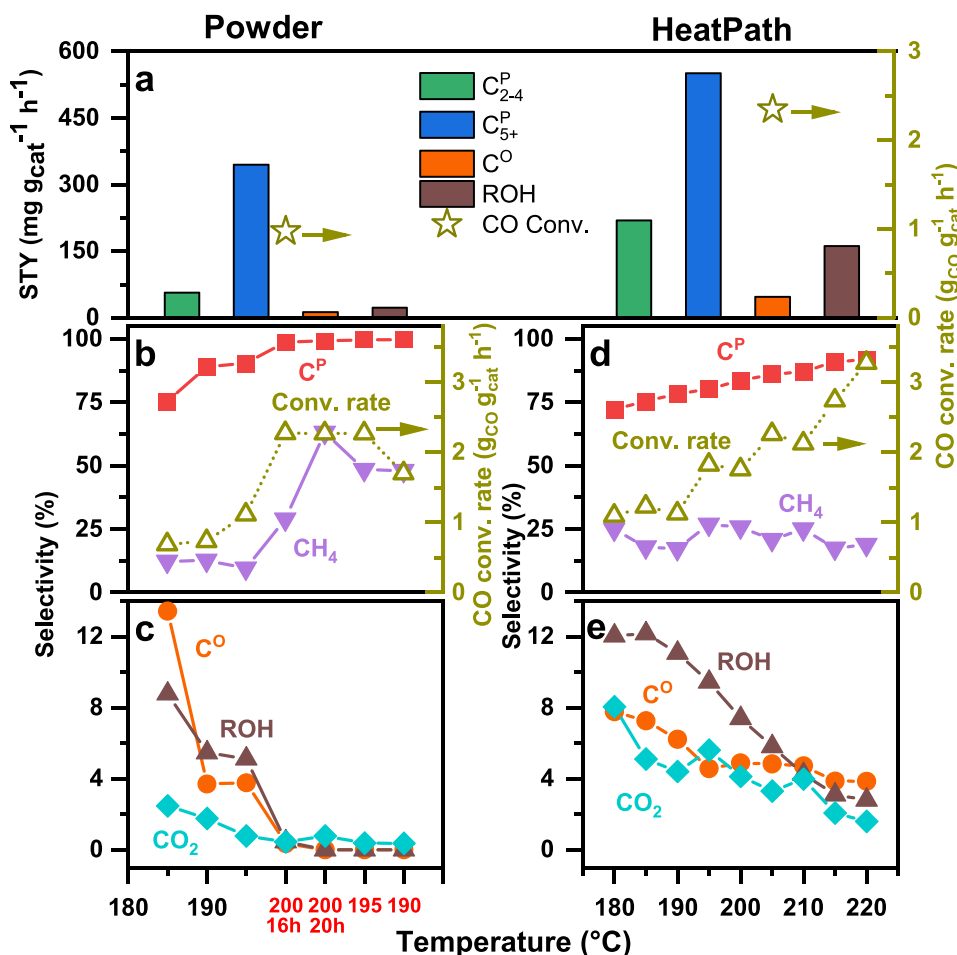


Fig. 2. Comparison of catalytic performance for powder and HeatPath catalysts at $P_{\text{total}} = 20$ bar, $H_2:CO = 2:1$, (a) CO conversion rate (CO Conv.) and STY of C_2 - C_4 paraffins (C_{2-4}^p), C_{5+} paraffins (C_{5+}^p), olefins (C^o), and alcohols (ROH) at 195 °C, $F_{\text{total}} = 30$ ml/min (STP), (b)-(e) CO conversion rate and product selectivity as a function of temperature from 180 °C to 220 °C with CO conversions controlled by adjusting feed gas flow rates.

(TOS) of 110 h for the powder catalyst and 131 h for the HeatPath catalyst. The feed gas mixture of H_2 and CO with $H_2/CO = 2$ was controlled at a flow rate of 30 ml/min (at standard temperature and pressure, STP). The results show that the HeatPath catalyst at equal temperature (195 °C) display a much higher CO conversion rate ($2.34 \text{ g}_{\text{CO}} \text{ g}_{\text{cat}}^{-1} \text{ h}^{-1}$ at 34.3 % CO conversion) compared to the powder catalyst ($0.97 \text{ g}_{\text{CO}} \text{ g}_{\text{cat}}^{-1} \text{ h}^{-1}$ at 57.3 % CO conversion), as well as a higher space time yield (STY) of C_{2-4} paraffins and alcohols, mainly methanol, ethanol, and 1-propanol (Table S2). Additionally, the HeatPath catalyst shows a much higher STY of C_{5+} paraffins (550.45 vs. $344.33 \text{ mg g}_{\text{cat}}^{-1} \text{ h}^{-1}$) and olefins (46.97 vs. $12.18 \text{ mg g}_{\text{cat}}^{-1} \text{ h}^{-1}$). These results highlight the significantly improved catalytic performance of the HeatPath catalyst.

The effect of temperature on both the powder and HeatPath catalysts was studied from 180 °C to 220 °C with a feed gas mixture of H_2 and CO ($H_2/CO = 2$). The gas flow rate was adjusted from 30 to 40 ml/min (STP) for the powder catalyst and 15–30 ml/min (STP) for the HeatPath catalyst to control the CO conversion (ranged from 32.0 % to 47.9 %). For the powder catalyst, as the temperature increased from 185 °C to 195 °C, the CO conversion rate increased from 0.69 to $0.97 \text{ g}_{\text{CO}} \text{ g}_{\text{cat}}^{-1} \text{ h}^{-1}$ (CO conversion from 40.4 % to 48.9 %), and the selectivity to olefins and alcohols decreased, while the CH_4 selectivity remained relatively constant at $\sim 12.5\%$, as shown in Fig. 2b and c. When the temperature was

further increased above 195 °C, a reaction run-away occurred only in the undiluted powder catalyst, as indicated by a nearly 100 % CO conversion or a CO conversion rate of $2.27 \text{ g}_{\text{CO}} \text{ g}_{\text{cat}}^{-1} \text{ h}^{-1}$. The CH_4 selectivity continuously increased from 28.9 % at 16 h TOS and 200 °C to 63.1 % at 20 h TOS for the same temperature.

When the powder catalyst temperature was subsequently lowered to 195 °C, the CO conversion remained at 100 % (CO conversion rate of $2.27 \text{ g}_{\text{CO}} \text{ g}_{\text{cat}}^{-1} \text{ h}^{-1}$) along with a high CH_4 selectivity of 48.5 %. Even further lowering the temperature to 190 °C did not lower the CH_4 selectivity (48.1 %) and still resulted in a CO conversion of about 100 % (CO conversion rate of $1.70 \text{ g}_{\text{CO}} \text{ g}_{\text{cat}}^{-1} \text{ h}^{-1}$). The powder catalyst performance before and after the reaction runaway near 200 °C was significantly different, as indicated through the CO conversion rate and CH_4 selectivity, as the powder catalyst deactivated due to the reaction runaway. Characterization of the spent powder catalyst by TEM (Fig. S3), XRD (Fig. S4), and Raman (Fig. S5 and Fig. S6) analysis showed the formation of Co aluminate spinel and graphitic carbon deposits on the spent powder catalysts.

In contrast, the HeatPath catalyst (Fig. 2d, e) did not experience a reaction runaway under any test conditions up to 260 °C, and its CO conversion rate increased with temperature up to 220 °C while the CH_4 selectivity remained relatively constant. The selectivity to alcohols, olefins, and CO_2 decreased with increasing temperature. At 220 °C, a CO

conversion rate of $3.28 \text{ g}_{\text{CO}} \text{ g}_{\text{cat}}^{-1} \text{ h}^{-1}$ (47.9 % CO conversion) was achieved along with a CH_4 selectivity of 18.9 %. Additionally, the advantage of the HeatPath catalyst in selectively enhancing C_{5+} paraffins production over CH_4 and C_{2-4} paraffins is evident in terms of the STY of products, as shown in Fig. S7.

3.3. The effects of H_2/CO ratio and temperature, as well as catalytic stability of the HeatPath catalyst during the Fischer–Tropsch reaction

The effect of the H_2/CO ratio on the performance of the HeatPath catalyst was first studied at 225°C . As seen in Fig. 3a, when the H_2/CO ratio increased from 1.2 to 2, the CO conversion increased from 54.6 to 67.2% while the CH_4 selectivity only slightly increased from 9.3 % to 13.8 %. This is in agreement with previous reports according to which higher H_2/CO ratios resulted in higher CH_4 selectivity [3,33,34]. The selectivity to paraffins, olefins, and alcohols remained relatively constant. The HeatPath core@shell catalyst was then studied at much lower H_2/CO ratios of 1 and 1.25 at 255°C (Fig. 3b). The gas flow rates were controlled at 80 and 90 ml/min (STP) for the runs with H_2/CO ratios of 1 and 1.25, respectively. A higher CO conversion (66.3%) was obtained at a H_2/CO ratio of 1.25 compared to 60.0 % at a H_2/CO ratio of 1, which corresponded to a slightly higher CO conversion rate (18.12 vs. $16.41 \text{ g}_{\text{CO}} \text{ g}_{\text{cat}}^{-1} \text{ h}^{-1}$). Slightly higher CH_4 selectivity was also obtained at a H_2/CO ratio of 1.25 compared to that at a H_2/CO ratio of 1. However, for both H_2/CO ratios, a very low CH_4 selectivity (<5 %) and a high C_{5+} selectivity (> 86 %) were achieved at 255°C . This is consistent with an alpha number of 0.83, as determined by the analysis of the liquid sample (Fig. S1, d) collected from the experiment with a H_2/CO ratio of 1. Additionally, a slightly higher selectivity to alcohols was observed at a lower H_2/CO ratio of 1.

To further evaluate the performance of the HeatPath catalyst and take advantage of its capabilities over a broad temperature range without the risk of reaction runaway, additional experiments were conducted from 230°C to 250°C with a H_2/CO ratio of 2 (Fig. 3c). The gas flow rate was adjusted between 56 and 140 ml/min (STP) to keep the CO conversion between 40.8 and 79.0 %. As the temperature increased from 230°C to 250°C , the CO conversion rate increased from 9.33 to $19.70 \text{ g}_{\text{CO}} \text{ g}_{\text{cat}}^{-1} \text{ h}^{-1}$, while keeping the CH_4 selectivity below 10 %. The selectivity to alcohols, olefins, and CO_2 remained relatively constant. A low CH_4 selectivity of <7 % even at 240°C and 245°C is consistent with high alpha numbers of 0.84 and 0.82, respectively, as determined by analyzing the liquid product (Fig. S1). Long-chain hydrocarbons up to C_{32} were detected in the liquid sample analysis. The high CO conversion rate of $19.70 \text{ g}_{\text{CO}} \text{ g}_{\text{cat}}^{-1} \text{ h}^{-1}$ achieved with the HeatPath catalyst is more than 20 times higher than that of the powder catalyst with the identical formulation, and it is accomplished without reaction runaway. Table S3 shows that, even without optimizing the pellet packing in the reactor, the volumetric CO conversion rate of the HeatPath catalyst ($0.43 \text{ g}_{\text{CO}} \text{ ml}_{\text{cat}/\text{bed}}^{-1} \text{ h}^{-1}$) is similar to that of the powder catalyst ($0.59 \text{ g}_{\text{CO}} \text{ ml}_{\text{cat}/\text{bed}}^{-1} \text{ h}^{-1}$), but it offers the added benefit of a much broader temperature range without sacrificing the selectivity to long-chain hydrocarbons.

To evaluate the stability of the HeatPath catalyst, its performance at two different TOS values of 259 h and 665 h was compared under identical reaction conditions (225°C , 20 bar, and a total gas flow rate of 30 ml/min (STP) with a H_2/CO ratio of 2 (Fig. 3d). It was found that even after studying the HeatPath catalyst at temperatures as high as 260°C and low H_2/CO ratios (as low as 1) over the 250 h TOS and 665 h TOS period without any regeneration, the CO conversion rate only decreased slightly, from 5.61 to $4.57 \text{ g}_{\text{CO}} \text{ g}_{\text{cat}}^{-1} \text{ h}^{-1}$ (CO conversion from

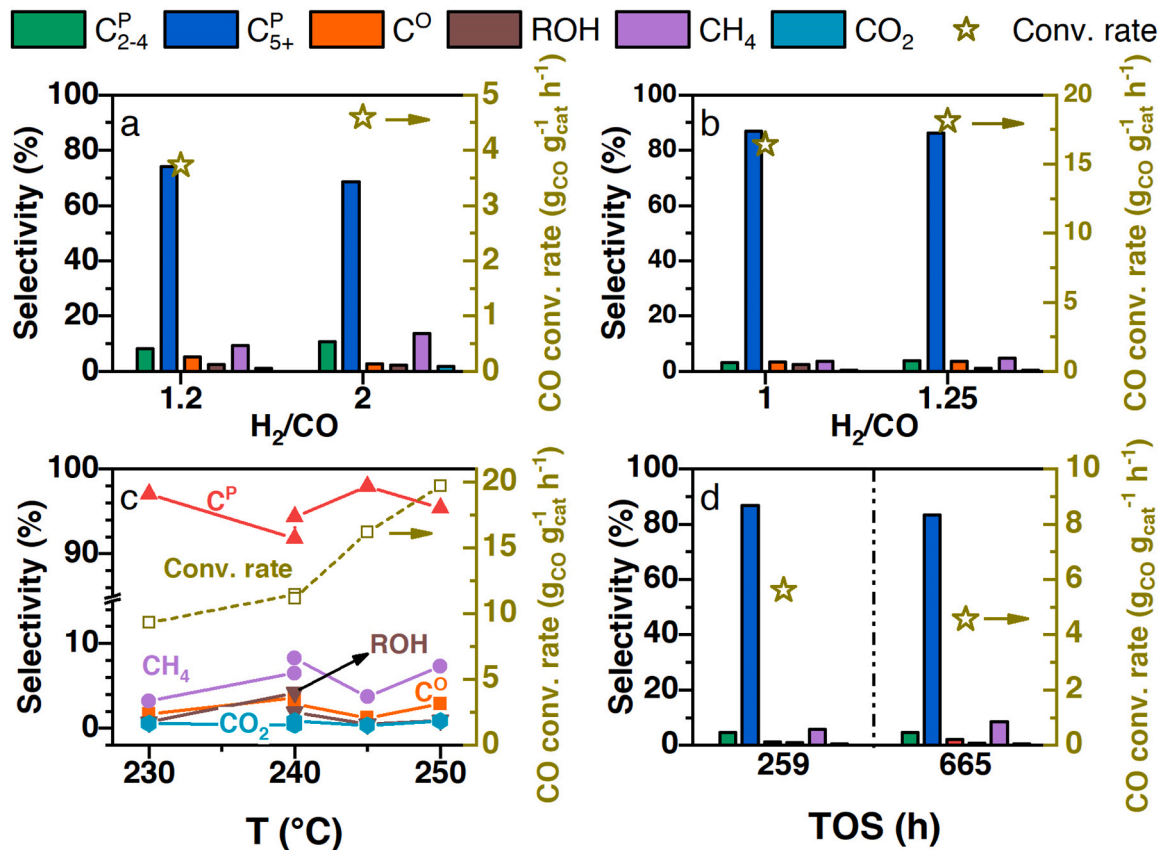


Fig. 3. Activity and selectivity of HeatPath $\text{SiC}@ \text{Co}/\text{Re}/\text{Al}_2\text{O}_3$ catalyst vs. (a) H_2/CO ratio at 225°C , (b) H_2/CO ratio at 255°C , (c) temperature at $\text{H}_2/\text{CO} = 1.8/1$, and (d) time at 225°C , 30 ml/min (STP), and $\text{H}_2/\text{CO} = 2$. Operated at 20 bar.

82.00 to 66.99 %), with minimal changes in product selectivity, including < 10 % CH₄ selectivity. This stability is supported by the results of the characterization for the spent HeatPath catalyst using TEM (Fig. S3), XRD (Fig. S4), and Raman (Fig. S5 and Fig. S6), which showed no signs of Co sintering, no Co₂AlO₄ formation, and significantly less carbon deposition compared to the spent powder catalyst.

4. Conclusions

In summary, a highly active Co-based catalyst, Co/Re/Al₂O₃, was coated with a uniform shell on to a commercially available HeatPath SiC-Al₂O₃ pellet support. The impact of the high thermal conductivity with the HeatPath core structure on the catalytic performance of the Co/Re/Al₂O₃ catalyst for the FTS reaction was investigated and found to significantly enhance the CO conversion rate and avoid the high-temperature runaway of the reaction. This improvement was attributed to the heat dissipation properties of the HeatPath SiC pellets, as demonstrated by the following key findings:

- (1) A simple “repeated dip and dry” process, without the use of binding or stabilizing materials, coated the active Co, Re, and Al species across the entire surface of the SiC pellet. Compared to the pristine powder Co/Re/Al₂O₃ catalyst, the coating by Co/Re/Al₂O₃ catalyst of the SiC pellet support prevented sintering of Co nanoparticles during the FTS reaction.
- (2) In the low temperature range (<200 °C), the coating of the HeatPath SiC-Al₂O₃ @ Co/Re/Al₂O₃ catalyst significantly improved the CO conversion rate and STY of hydrocarbon products, particularly C₂₋₄ paraffins and C₅₊ paraffins. This superiority of the HeatPath SiC-Al₂O₃ @ Co/Re/Al₂O₃ catalyst became even more evident as the temperature increased to 200 °C and above. Starting at 195 °C, the powder Co/Re/Al₂O₃ catalyst showed irreversible deactivation within the first few hours, while the HeatPath catalyst maintained high selectivity towards C₅₊ paraffins with a slightly reduced CO conversion rate for over 660 h, even at temperatures as high as 260 °C.
- (3) At a constant H₂/CO ratio of 1.8, as the temperature increased from 230° to 250°C, the CO conversion rate increased from 9.33 to 19.70 g_{CO} g_{cat}⁻¹ h⁻¹, while CH₄ selectivity remained constantly below 10 %. The selectivity to alcohols, olefins, and CO₂ remained relatively constant. Additionally, even higher CO conversion rates and higher C₅₊ yields were achieved with only a slight increase in CH₄ selectivity (up to 14 %) at higher H₂/CO ratios, highlighting the robustness of the HeatPath catalyst across a wide range of temperatures and H₂/CO ratios.
- (4) Compared to the published literature on Co-based catalysts (Table S4), the present HeatPath core SiC-Al₂O₃ @shell (Co/Re/Al₂O₃) exhibits exceptional catalytic performance, characterized by its highest C₅₊ selectivity (91 %) compared to reported Co-based catalysts by effectively suppressing CH₄ and CO₂ production while maintaining high activity (68.2 % conversion). These results demonstrate the potential to efficiently synthesize fuels through FTS using this facile and efficient approach for catalyst design, which is conducive for large-scale application. Future study will provide in-depth understanding of the factors/reasons that lead to the significant improvement on the catalyst performance of pellet catalysts. The HeatPath structure may also be extended to other highly endothermic or exothermic reactions, such as the dry-reforming of CO₂ with methane, selective oxidation of alkanes, and others.

CRedit authorship contribution statement

Rui Zhang: Investigation, Methodology, Writing – original draft. **Junrui Li:** Investigation, Methodology, Writing – original draft. **Anna Lee Tonkovich:** Formal analysis, Writing – review & editing. **Cody Lockhart:** Methodology, Writing – review & editing. **Xiaoyan Wang:** Methodology, Data curation. **Wenda Hu:** Methodology, Writing – review & editing. **Hafsa Karroum:** Methodology, Data curation. **Matthew Seabaugh:** Discussion, Writing - review & editing. **Norbert Kruse:** Supervision, Writing – review & editing. **Yong Wang:** Conceptualization, Writing – review & editing, Supervision.

Declaration of Competing Interest

The authors declare that they have no known competing financial interests or personal relationships that could have appeared to influence the work reported in this manuscript.

Data Availability

Data will be made available on request.

Acknowledgements

The authors thank Nexceris and the US Department of Energy for providing funding to conduct the research. TEM was conducted using FEI Technai G2 20 Twin in the Franceschi Microscopy and Imaging Center (FMIC), Washington State University. R.Z. was partly supported by a Chambroad Scholarship for pursuing his Ph.D studies.

Appendix A. Supporting information

Supplementary data associated with this article can be found in the online version at doi:10.1016/j.apcata.2023.119419.

References

- [1] M. Rahmati, M.S. Safdari, T.H. Fletcher, M.D. Argyle, C.H. Bartholomew, *Chem. Rev.* 120 (2020) 4455–4533.
- [2] J.C. Mohandas, M.K. Gnanamani, G. Jacobs, W. Ma, Y. Ji, S. Khalid, B.H. Davis, *ACS Catal.* 1 (2011) 1581–1588.
- [3] S. Lögdberg, M. Lualdi, S. Järs, J.C. Walmsley, E.A. Blekkan, E. Rytter, A. Holmen, *J. Catal.* 274 (2010) 84–98.
- [4] H. Schulz, *Catal. Today* 228 (2014) 113–122.
- [5] B. Ernst, L. Hilaire, A. Kiennemann, *Catal. Today* 50 (1999) 413–427.
- [6] Y. Xiang, R. Barbosa, N. Kruse, *ACS Catal.* 4 (2014) 2792–2800.
- [7] Y. Xiang, N. Kruse, *Nat. Commun.* 7 (1) (2016) 6.
- [8] I.K. Van Ravenhorst, A.S. Hoffman, C. Vogt, A. Boubnov, N. Patra, R. Oord, C. Akatay, F. Meirer, S.R. Bare, B.M. Weckhuysen, *ACS Catal.* 11 (2021) 2956–2967.
- [9] Z. Zhu, G. Lu, Z. Zhang, Y. Guo, Y. Guo, Y. Wang, *ACS Catal.* 3 (2013) 1154–1164.
- [10] L. Zhong, F. Yu, Y. An, Y. Zhao, Y. Sun, Z. Li, T. Lin, Y. Lin, X. Qi, Y. Dai, L. Gu, J. Hu, S. Jin, Q. Shen, H. Wang, *Nature* 538 (2016) 84–87.
- [11] J. Li, Y. He, L. Tan, P. Zhang, X. Peng, A. Oruganti, G. Yang, H. Abe, Y. Wang, N. Tsubaki, *Nat. Catal.* 1 (2018) 787–793.
- [12] R. Zhang, L. Kang, H. Liu, B. Wang, D. Li, M. Fan, *Appl. Catal. B Environ.* 269 (2020), 118847.
- [13] J. van de Loosdrecht, B. Balzhinimaev, J.A. Dalmon, J.W. Niemantsverdriet, S. V. Tsybulya, A.M. Saib, P.J. van Berge, J.L. Visagie, *Catal. Today* 123 (2007) 293–302.
- [14] B. Jongsomjit, J. Panpranot, J.G. Goodwin, *J. Catal.* 204 (2001) 98–109.
- [15] S.T. Sie, R. Krishna, *Appl. Catal. A Gen.* 186 (1999) 55–70.
- [16] R. Guettel, U. Kunz, T. Turek, *Chem. Eng. Technol.* 31 (2008) 746–754.
- [17] G. Jacobs, B.H. Davis, *Multiph. Catal. React. Theory Des. Manuf. Appl.* (2016) 269–294.
- [18] W. Liu, Y. Wang, W. Wilcox, S. Li, *AIChE J.* 58 (2012) 2820–2829.
- [19] C. Cao, J. Hu, S. Li, W. Wilcox, Y. Wang, *Catal. Today* 140 (2009) 149–156.
- [20] S.R. Deshmukh, A.L.Y. Tonkovich, K.T. Jarosch, L. Schrader, S.P. Fitzgerald, D. R. Kilanowski, J.J. Lerou, T.J. Mazanec, *Ind. Eng. Chem. Res.* 49 (2010) 10883–10888.

- [21] J.C. Park, N.S. Roh, D.H. Chun, H. Jung, J.I. Yang, *Fuel Process. Technol.* 119 (2014) 60–66.
- [22] L. Fratalocchi, C.G. Visconti, G. Groppi, L. Lietti, E. Tronconi, *Chem. Eng. J.* 349 (2018) 829–837.
- [23] J. Harmel, L. Peres, M. Estrader, A. Berliet, S. Maury, A. Fécant, B. Chaudret, P. Serp, K. Soulantica, *Angew. Chem. - Int. Ed.* 57 (2018) 10579–10583.
- [24] E. Ranjbarnodeh, S. Serajzadeh, A.H. Kokabi, A. Fischer, *J. Mater. Sci.* 46 (2011) 3225–3232.
- [25] T. Fishedick, M. Kind, B. Dietrich, *Int. J. Therm. Sci.* 96 (2015) 1–11.
- [26] J. Banhart, *Prog. Mater. Sci.* 46 (2001) 559–632.
- [27] P. Nguyen, C. Pham, *Appl. Catal. A Gen.* 391 (2011) 443–454.
- [28] V. Iablokov, S.A. Alekseev, S. Gryn, I. Bezverkhyy, V. Zaitsev, L. Kovarik, T. Visart de Bocarme, N. Kruse, *J. Catal.* 383 (2020) 297–303.
- [29] M. Lacroix, L. Dreibine, B. De Tymowski, F. Vigneron, D. Edouard, D. Bégin, P. Nguyen, C. Pham, S. Savin-Poncet, F. Luck, M.J. Ledoux, C. Pham-Huu, *Appl. Catal. A Gen.* 397 (2011) 62–72.
- [30] Y. Liu, B. De Tymowski, F. Vigneron, I. Florea, O. Ersen, C. Meny, P. Nguyen, C. Pham, F. Luck, C. Pham-Huu, *ACS Catal.* 3 (2013) 393–404.
- [31] Y. Liu, O. Ersen, C. Meny, F. Luck, C. Pham-Huu, *ChemSusChem* 7 (2014) 1218–1239.
- [32] X. Lu, D. Hildebrandt, D. Glasser, *Appl. Catal. A Gen.* 506 (2015) 67–76.
- [33] D. Tristantini, S. Lögdberg, B. Gevert, Ø. Borg, A. Holmen, *Fuel Process. Technol.* 88 (2007) 643–649.
- [34] O. Akbarzadeh, N.A.M. Zabidi, G. Wang, A. Kordijazi, H. Sadabadi, S. Moosavi, A. A. Babadi, N.A. Hamizi, Y.A. Wahab, M. Ab Rahman, S. Sagadevan, Z. Z. Chowdhury, M.R. Johan, *Symmetry (Basel)* 12 (2020) 698.